Supplemental Information

Integrative Structure-Function Mapping of the Nucleoporin Nup133 Suggests a Conserved Mechanism for Membrane Anchoring of the Nuclear Pore Complex

Seung Joong Kim[1]*, Javier Fernandez-Martinez[2]*, Parthasarathy Sampathkumar[3]*, Anne Martel[4], Tsutomu Matsui[4], Hiro Tsuruta[4], Thomas M. Weiss[4], Yi Shi[5], Ane Markina-Inarrairaegui[6], Jeffery B. Bonanno[3], J. Michael Sauder[7], Stephen K. Burley[8], Brian T. Chait[5], Steven C. Almo[3], Michael P. Rout[2], and Andrej Sali[1]

1. Department of Bioengineering and Therapeutic Sciences, Department of Pharmaceutical Chemistry, California Institute for Quantitative Biosciences, Byers Hall, 1700 4th Street, Suite 503B, University of California, San Francisco, San Francisco, CA 94158, USA

2. Laboratory of Cellular and Structural Biology, The Rockefeller University, New York, NY 10065, USA

3. Department of Biochemistry, Ullmann Building, Room 409, Albert Einstein College of Medicine, 1300 Morris Park Avenue, Bronx, NY 10461, USA

4. Stanford Synchrotron Radiation Lightsource, SLAC National Accelerator Laboratory, 2575 Sand Hill Road, MS 69, Menlo Park, CA 94025, USA

5. Laboratory of Mass Spectrometry and Gaseous Ion Chemistry, The Rockefeller University, New York, NY 10065, USA

6. Laboratorio de Genetica Molecular de Aspergillus, Departamento de Biología Celular y Molecular, Centro de Investigaciones Biológicas (CSIC). Ramiro de Maeztu 9, 28040,

Madrid, Spain.

7. Discovery Chemistry Research and Technologies (DCR&T), Eli Lilly and Company, Lilly Biotechnology Center, 10300 Campus Point Drive, Suite 200, San Diego, CA 92121, USA

8. Center for Integrative Proteomics Research, Department of Chemistry and Chemical Biology, Rutgers, The State University of New Jersey, 174 Frelinghuysen Road, Piscataway, NJ 08854, USA

**These authors contributed equally to this work as co-first authors.*

Corresponding authors

Steven C. Almo, Department of Biochemistry, Ullmann Building, Room 409, Albert Einstein College of Medicine, 1300 Morris Park Avenue, Bronx, NY 10461, USA.

tel: +1 718 4302746; fax: +1 718 430 8565; steve.almo@einstein.yu.edu

Michael. P. Rout, Box 213, Laboratory of Cellular and Structural Biology, Rockefeller University, 1230 York Avenue, New York, NY10021, USA.

tel: +1 212 327 8135; fax: +1 212 327 7193; rout@rockefeller.edu

Andrej Sali, UCSF MC 2552, Byers Hall at Mission Bay, Suite 503B, University of California, San Francisco, 1700 4th Street, San Francisco, CA 94158, USA

tel: +1 415 514 4227; fax: +1 415 514 4231; sali@salilab.org

Supplemental Experimental Procedures

Cloning, expression, and purification of *Sc*Nup133 and *Vp*Nup133 constructs

The genes encoding of *Saccharomyces cerevisiae* Nup133 (*Sc*Nup133) constructs were cloned from the genomic DNA of the yeast strain Sc2601D-5 (American Type Culture Collection, USA). The desired truncations were PCR amplified using appropriate forward and reverse primers. Similarly, the gene encoding N-terminal domain of *Vanderwaltozyma polyspora* Nup133 covering residues 55 to 502 [*Vp*Nup133$^{55\text{-}502}$] was cloned from *Vanderwaltozyma polyspora* (strain DSM 70294 / ATCC 22028) genomic DNA. The purified PCR product were subsequently TOPO® (Invitrogen, USA) cloned into pSGX3, a derivative of pET26b(+), giving rise to proteins with a non-cleavable C-terminal hexa histidine tag. The resulting plasmid was transformed into BL21(DE3)-Condon+RIL (Invitrogen, USA) cells for overexpression. Expression of Se-Met protein (1) was carried out in 1 L of HY media at 22ºC containing 50 µg/ml of kanamycin and 35 µg/ml of chloramphenicol. Protein expression was induced by addition of 0.4 mM IPTG. Cells were harvested after 21 hours by centrifugation at 4ºC. For purification, the E. coli cell pellet was resuspended in 30 mL of cold buffer containing 20 mM Tris HCl pH 8.0, 500 mM NaCl, 25 mM imidazole, and 0.1% (v/v) Tween20 and cells were lysed via sonication. Debris was removed by centrifugation at 4ºC. The decanted supernatant was applied to a 5 mL HisTrapHP column (GE Health Care, USA) charged with nickel and pre-equilibrated with 20 mM Tris HCl pH 8.0, 500 mM NaCl, 10% (v/v) glycerol, and 25 mM imidazole. The sample was washed with 5 column volumes (CV) of 20 mM Tris HCl pH 8.0, 500 mM NaCl, 10% (v/v) glycerol, and 40 mM imidazole and subsequently eluted with 2 CV of same

buffer with an imidazole concentration of 250 mM. Eluted protein was passed over a 120 mL Superdex 200 size exclusion column equilibrated with 10 mM HEPES pH 7.5, 150 mM NaCl, 10% (v/v) glycerol, and 5 mM DTT (protein storage buffer). SDS-PAGE analysis showed greater than 95% purity and protein fractions corresponding to the symmetric portion of the size exclusion chromatography profile were pooled for concentration using AMICON spin filters. Concentrated protein aliquots were frozen in liquid nitrogen and stored at -80ºC.

Small angle X-ray Scattering (SAXS)

SAXS measurements of 18 constructs of *Sc*Nup133 and one construct of *Vp*Nup133N$^{55\text{-}502}$ (Supplemental Figures S3 and S4, and Supplemental Table S1) were carried out both at Beamline 4-2 of the Stanford Synchrotron Radiation Lightsource (SSRL) in the SLAC National Accelerator Laboratory and at SIBYLS Beamline 12.3.1 of the Advanced Light Source (ALS) in the Lawrence Berkeley National Laboratory (LBNL). All protein samples for SAXS were suspended in the protein storage buffer, composed of 20 mM HEPES at pH 8.0, 500 mM NaCl, 10 % (v/v) glycerol, and 5 mM DTT containing four complete protease inhibitor tablets in 400 mL. All the suspensions were filtered through 0.1 µm membranes (Millipore, Bedford, MA) and a total of 10% glycerol was added to reduce radiation damage (2).

At SSRL, the beam energy and current were 11 keV and 200 mA, respectively. A silver behenate sample was used to calibrate the q-range and detector distance. Data collection was controlled with Blu-Ice (3). We used an automatic sample delivery system equipped with a 1.5 mm-diameter thin-wall quartz capillary within which a sample

aliquot was oscillated in the X-ray beam to minimize radiation damage (4). The sample was placed at 1.7 meter from a MX225-HE (Rayonix, USA) CCD detector with a binned pixel size of 293 μm by 293 μm. Ten to 24 1-3 sec exposures were made for each protein sample maintained at 15ºC. Each of the diffraction images was scaled using the transmitted beam intensity, azimuthally integrated by SASTool (http://ssrl.slac.stanford.edu/~saxs/analysis/sastool.htm, formarly called MarParse), and averaged to obtain fully processed data in the form of intensity versus q [$q=4\pi\sin(\theta)/\lambda$, θ=one-half of the scattering angle; λ=X-ray wavelength]. The buffer profile was obtained in the same manner and subtracted from a protein profile.

At ALS, samples were prepared on a 96-well plate and kept at 10^{o}C until SAXS measurement. An automatic sample delivery system equipped with a Hamilton pipetting robot was used (5). SAXS data were collected on a MAR165 area detector (Rayonix, USA), placed at 1.5 m from the SAXS sample cell. Exposures of 2 sec/10 sec/2 sec were made in series for each protein sample maintained at 10^{o}C. The SAXS data obtained at ALS were processed identically to the SSRL data, by using the ogreNew software.

The average of the lower scattering angle parts ($q < 0.15$ Å^{-1}) of the lower concentration profiles (0.5-1.0 mg/mL) and the average of the higher scattering angle parts ($q > 0.12$ Å^{-1}) of the higher concentration (1.5-5.0 or higher mg/mL) profiles were merged to obtain the final experimental SAXS profiles.

Negative-stain electron microscopy (EM) of *Sc*Nup133$^{2-1157}$

A 2.5 ml drop of purified recombinant *Sc*Nup133$^{2-1157}$ at concentration of 0.05

mg/ml was applied to glow-discharged carbon-coated copper grids. The grids were washed with two drops of deionized water and rinsed with two drops of freshly prepared 0.75% uranyl formate, then stained for a minute and air-dried. The EM images of *Sc*Nup133$^{2\text{-}1157}$ were collected at room temperature on a Philips Tecnai T20 (FEI Inc., USA) transmission electron microscope operating at an accelerating voltage of 200 kV at 50,000x magnification and underfocus ~1 µm. Images were recorded on a 2048 × 2048 CCD camera (Gatan Megascan 795, 30 µm pixel size) using a camera length of 3000 mm and a selected area aperture of 70 µm (6). The pixel size at the specimen level was 2.28739 Å. 1976 individual particles were selected interactively from images using Boxer from EMAN (7), and windowed into individual particle images with a size of 120x120 pixels. The side length of the images was chosen to be approximately twice the length of the longest particle dimension. The contrast transfer function (CTF) of the images was determined using ctfit from EMAN and the phases flipped accordingly. The particles were normalized and subjected to the *Iterative Stable Alignment and Clustering* (ISAC) (8) method to produce stable 2D class averages, resulting in 1530 particles selected for 23 stable class averages (Figure 3C). The program was run iteratively for 10 generations in total; after each generation, stable particles were removed from the stack and the program was re-run with unclassified particles until no new classes were found. A pixel error (*thld_err*) of $2\sqrt{3}$ was used for the stability threshold. The other parameters used for running ISAC are *img_per_grp* (number of images per class in the ideal case) of 150 and *ou* (outer ring of the resampling to polar coordinates) of 30.

Conformational Sampling using *AllosMod*

The initial model of *Sc*Nup133$^{2\text{-}1157}$ was subjected to molecular dynamics-based conformational sampling, using *AllosMod* (http://salilab.org/allosmod) (9). We repeated *AllosMod* 7 times with varying input parameter sets of MDTEMP, DEVIATION and LOCALRIGID, and each of the 7 runs generated 1,000 conformations independently; MDTEMP is the temperature (in degrees Kelvin) for the simulation; DEVIATION is the distance (in Ångstroms) that the atoms will be randomized when creating the initial structure; LOCALRIGID is a value of True or False. If set to True, secondary structure, corresponding to the input PDB files, will have increased stability in the simulation. Increased stability is maintained by increasing the energy by a factor of 10 for all C alpha-C alpha contacts between 2 and 5 residues apart. The parameter sets for each of the 7 independent *AllosMod* runs are summarized, as follows.

1st run of Basic 300K: MDTEMP = 300, DEVIATION = 5, LOCALRIGID = False

2nd run of Basic 310K: MDTEMP = 310, DEVIATION = 5, LOCALRIGID = False

3rd run of Basic 320K: MDTEMP = 320, DEVIATION = 5, LOCALRIGID = False

4th run of Basic 350K: MDTEMP = 350, DEVIATION = 5, LOCALRIGID = False

5th run of Intermediate 300K: MDTEMP = 300, DEVIATION = 10, LOCALRIGID = True

6th run of Intermediate 325K: MDTEMP = 325, DEVIATION = 10, LOCALRIGID = True

7th run of Intermediate 350K: MDTEMP = 350, DEVIATION = 10, LOCALRIGID = True

Files for the input data, script, and output models are available at http://salilab.org/nup133.

Annotating the potential ArfGAP1 lipid packing sensor (ALPS) motifs

We annotated 5 potential ALPS motifs in the β-propeller N-terminal domain for *Hs*Nup133 (Supplemental Figure S2A), *Vp*Nup133 (Supplemental Figure S2B), *Sc*Nup133 (Supplemental Figure S2C), and *Sc*Nup120 (Supplemental Figures S2 D-E). The potential ALPS motifs (red) are visualized in their corresponding structures (gray) using UCSF Chimera (10), and highlighted by the blue circles. The helical-wheel representations of the potential ALPS motifs are also shown, with an arrow in the center of the helical-wheel representing the direction and strength of the mean hydrophobic moment of the corresponding ALPS motif. Each table in the Supplemental Figure S2 A-E was generated on the HeliQuest web-server (11), summarizing the physico-chemical properties and the contents of the polar residues and non-polar residues, as well as the hydrophoboic face in the corresponding ALPS motif.

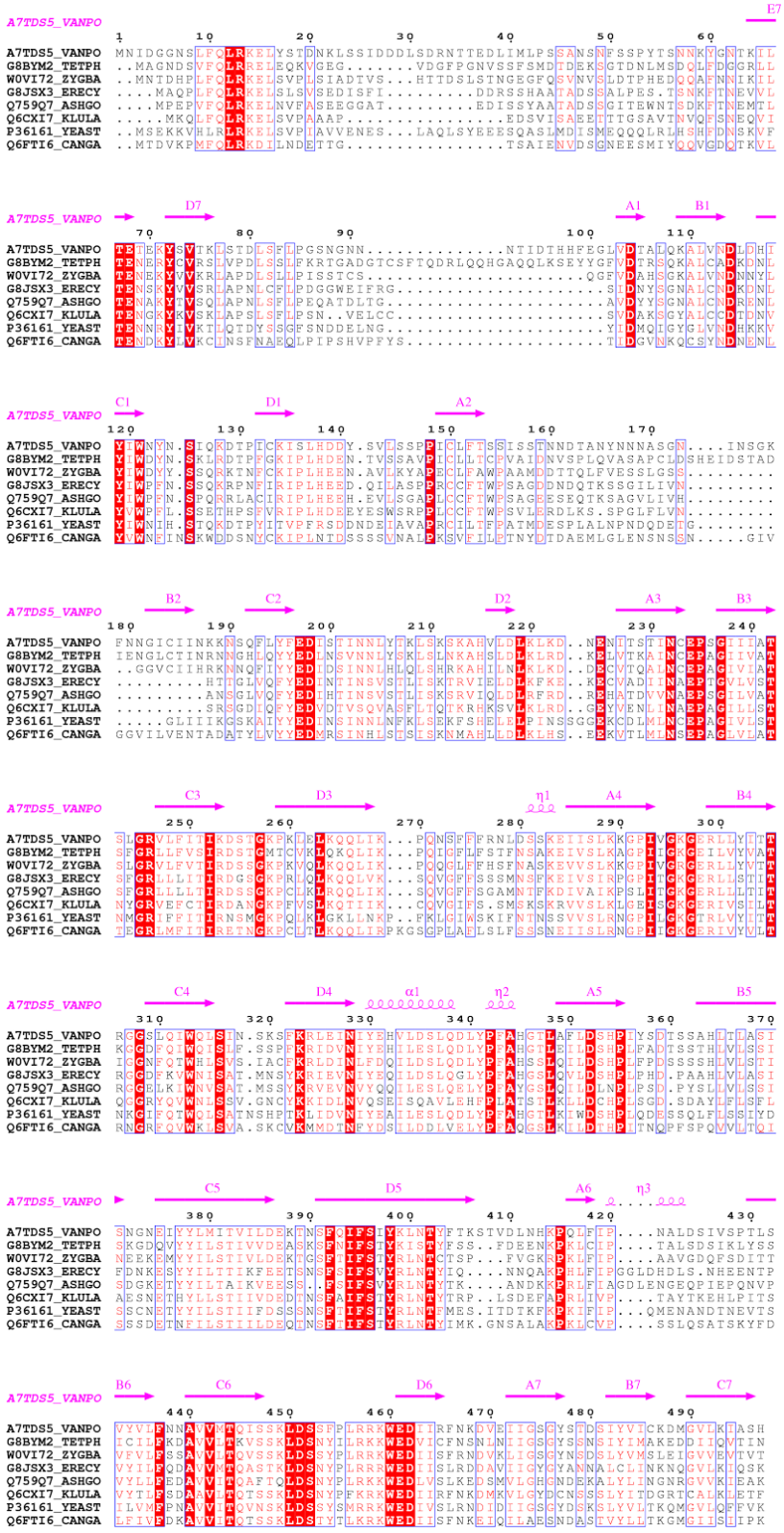

Supplemental Figure S1. Sequence alignment of the 8 fungal Nup133s

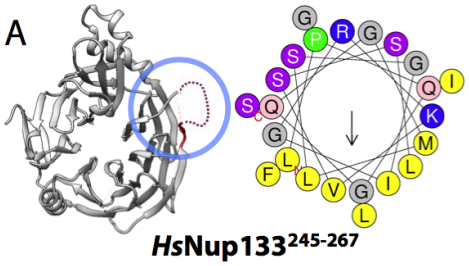

*Hs*Nup133$^{245-267}$

LPQGQGMLSGIGRKVSSLFGILS

Physico-chemical properties	Polar residues + GLY	Nonpolar residues
Hydrophobicity <H>	Polar residues + GLY (n / %)	Nonpolar residues (n / %)
0.555	13 / 56.52	10 / 43.48
Hydrophobic moment <μH>	Uncharged residues + GLY	Aromatic residues
0.417	GLN 2, SER 4, GLY 5	PHE 1,
Net charge z	Charged residues	Special residues
2	LYS 1, ARG 1,	CYS 0, PRO 1
Hydrophobic face : M L I G L V L L F		

Supplemental Figure S2 (A). The ALPS motif of *Hs*Nup133$^{245-267}$ and its property

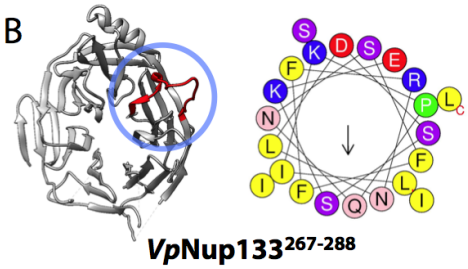

*Vp*Nup133$^{267-288}$

LIKPQNSFFFRNLDSSKEIISL

Physico-chemical properties	Polar residues + GLY	Nonpolar residues
Hydrophobicity <H>	Polar residues + GLY (n / %)	Nonpolar residues (n / %)
0.482	12 / 54.55	10 / 45.45
Hydrophobic moment <μH>	Uncharged residues + GLY	Aromatic residues
0.355	GLN 1, SER 4, ASN 2, GLY 0	PHE 3,
Net charge z	Charged residues	Special residues
1	LYS 2, ARG 1, GLU 1, ASP 1,	CYS 0, PRO 1
Hydrophobic face : F I I L		

Supplemental Figure S2 (B). The potential ALPS motif of *Vp*Nup133$^{267-288}$ and its property

C

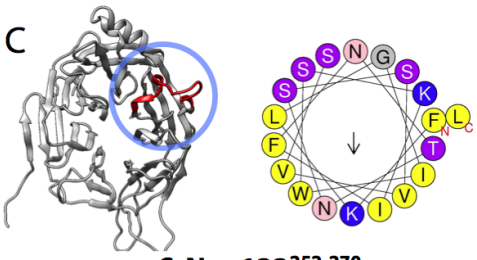

***Sc*Nup133$^{252\text{-}270}$**

FKLGIWSKIFNTNSSVVSL

Physico-chemical properties	Polar residues + GLY	Nonpolar residues
Hydrophobicity <H>	**Polar residues + GLY (n / %)**	**Nonpolar residues (n / %)**
0.642	10 / 52.63	9 / 47.37
Hydrophobic moment <μH>	**Uncharged residues + GLY**	**Aromatic residues**
0.262	SER 4, THR 1, ASN 2, GLY 1	TRP 1, PHE 2,
Net charge z	**Charged residues**	**Special residues**
2	LYS 2,	CYS 0, PRO 0
Hydrophobic face : W V F L		

Supplemental Figure S2 (C). The potential ALPS motif of *Sc*Nup133$^{252\text{-}270}$ and its property

D

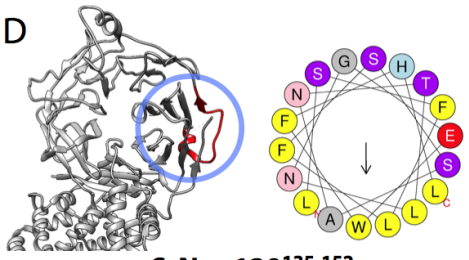

***Sc*Nup120$^{135\text{-}152}$**

LSFLFSSANTLNGEWFHL

Physico-chemical properties	Polar residues + GLY	Nonpolar residues
Hydrophobicity <H>	**Polar residues + GLY (n / %)**	**Nonpolar residues (n / %)**
0.731	9 / 50.00	9 / 50.00
Hydrophobic moment <μH>	**Uncharged residues + GLY**	**Aromatic residues**
0.365	HIS 1, SER 3, THR 1, ASN 2, GLY 1	TRP 1, PHE 3,
Net charge z	**Charged residues**	**Special residues**
-1	GLU 1,	CYS 0, PRO 0
Hydrophobic face : L L L W A L		

Supplemental Figure S2 (D). The potential ALPS motif of *Sc*Nup120$^{135\text{-}152}$ and its property

E

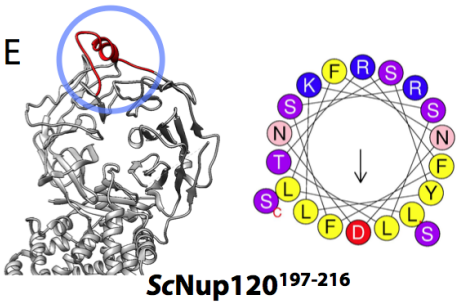

*Sc*Nup120$^{197\text{-}216}$

LLFNDNSYLKSLTRFFSRSS

Physico-chemical properties	Polar residues + GLY	Nonpolar residues
Hydrophobicity <H>	**Polar residues + GLY (n / %)**	**Nonpolar residues (n / %)**
0.411	12 / 60.00	8 / 40.00
Hydrophobic moment <μH>	**Uncharged residues + GLY**	**Aromatic residues**
0.395	SER 5, THR 1, ASN 2, GLY 0	TYR 1, PHE 3,
Net charge z	**Charged residues**	**Special residues**
2	LYS 1, ARG 2, ASP 1,	CYS 0, PRO 0
Hydrophobic face : F L		

Supplemental Figure S2 (E). The potential ALPS motif of *Sc*Nup120$^{197\text{-}216}$ and its property

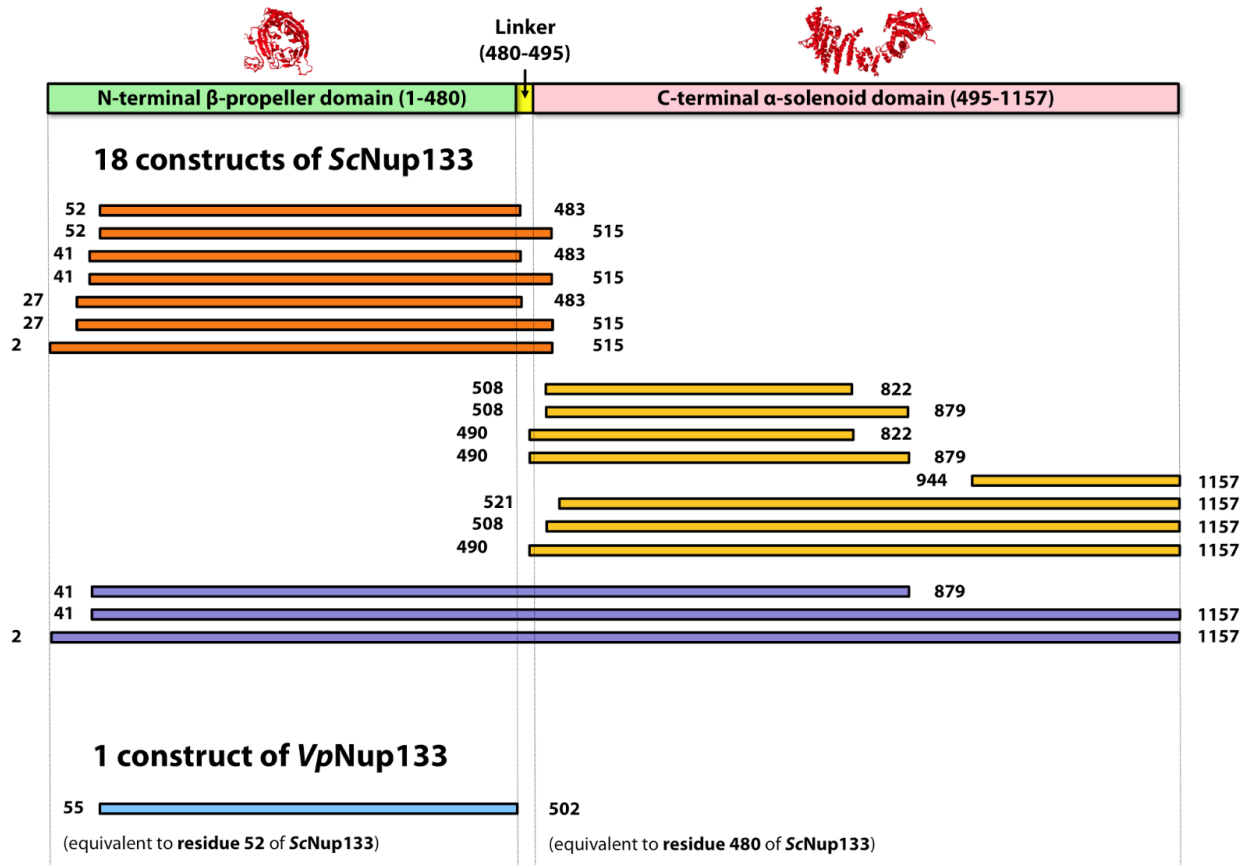

Supplemental Figure S3. The schematic construct design of *Vp* and *Sc*Nup133

Nup133 is divided into the N-terminal β-propeller and the C-terminal α-solenoid domains, in an iterative manual process relying on predicted secondary structure, gaps in multiple sequence alignments, and sequence–structure alignment by threading (12). We cloned, expressed, and purified the resulting 18 constructs of *Sc*Nup133; 7 constructs (bars in red) covering the N-terminal domain, 8 constructs (bars in yellow) covering the C-terminal domain, and 3 remaining constructs (bars in violet) covering the both domains partially or entirely. The N-terminal domain of *Vanderwaltozyma polyspora* Nup133 covering residues 55 to 502 (*Vp*Nup133$^{55\text{-}502}$) was also cloned, expressed, and purified.

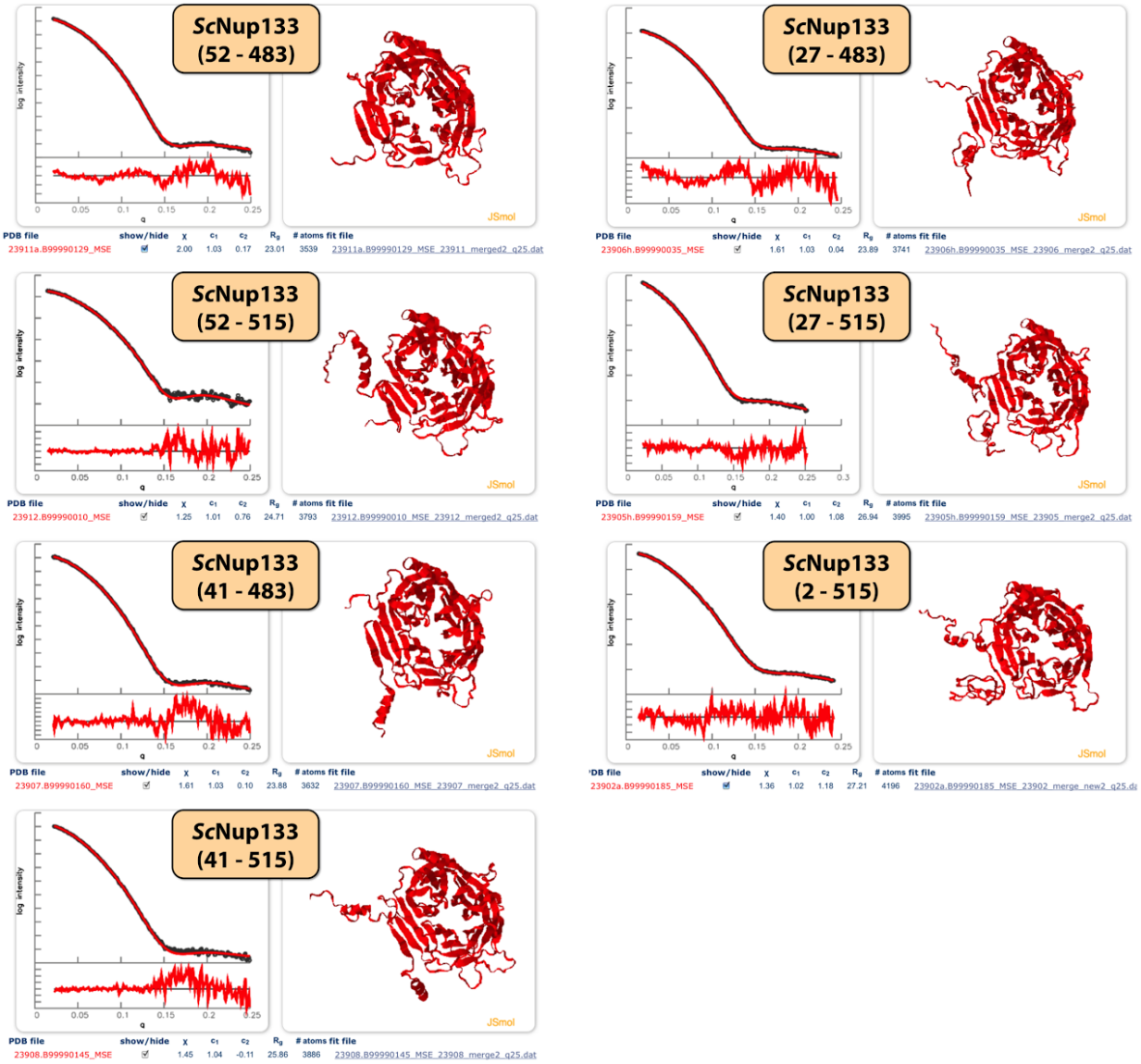

Supplemental Figure S4 (A). Summary of SAXS profiles for 18 nested *Sc*Nup133 constructs (N-terminal β-propellers).

The plots were prepared by FoXS webserver (http://salilab.org/foxs) (13, 14). For each construct, the structure shown is the best-scoring model. The residual (experimental intensity / calculated intensity) plot is also shown below the corresponding SAXS profile.

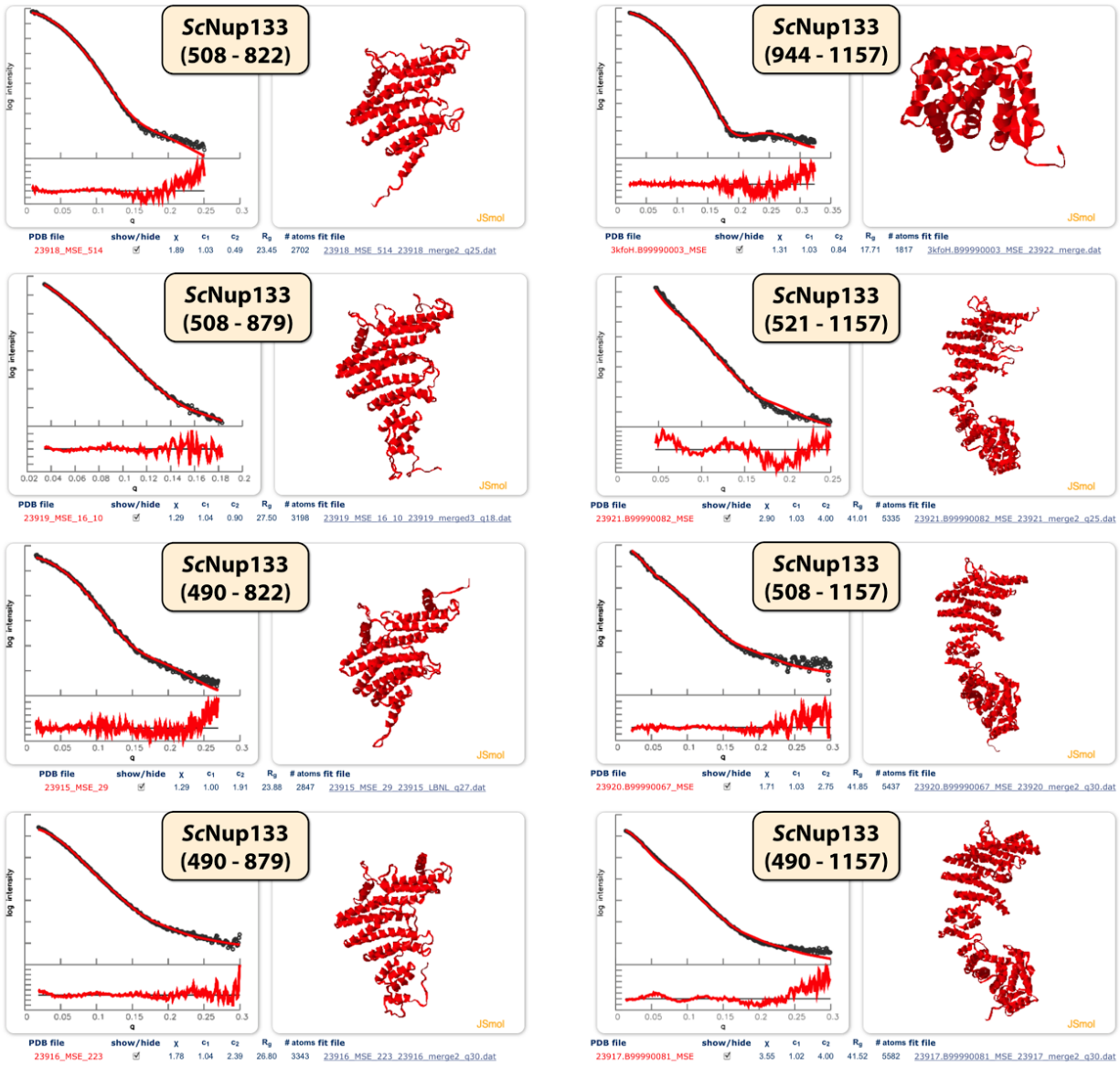

Supplemental Figure S4 (B). Summary of SAXS profiles for 18 nested *Sc*Nup133 constructs (C-terminal α-solenoids).

See the legend for Supplemental Figure S4 (A)

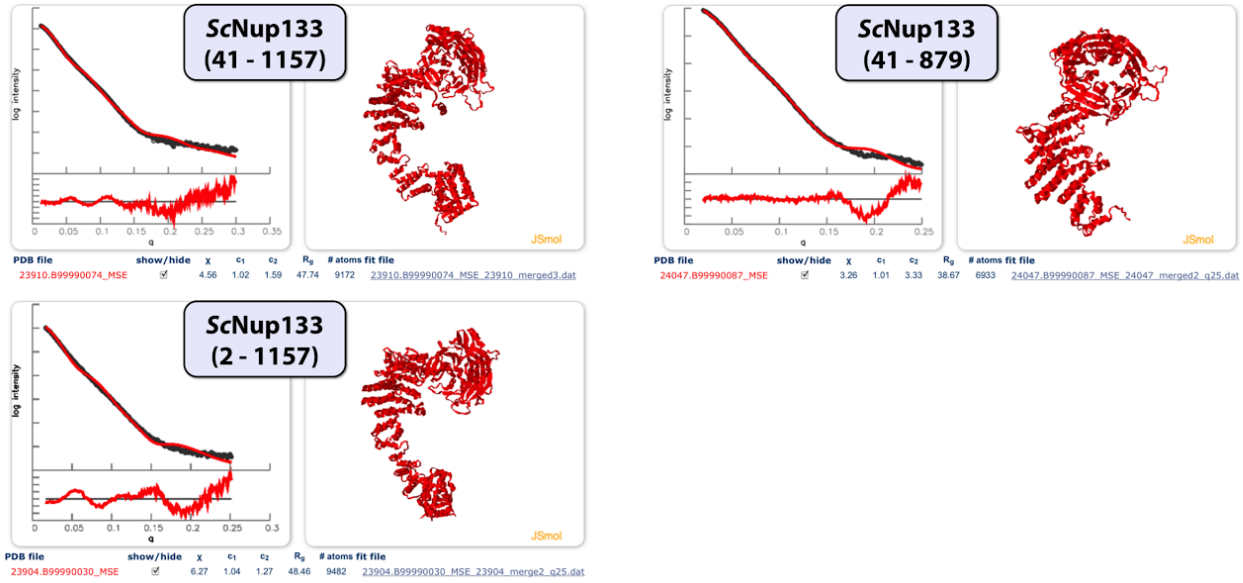

Supplemental Figure S4 (C). Summary of SAXS profiles for 18 nested *Sc*Nup133 constructs (N-terminal β-propellers + C-terminal α-solenoids)

See the legend for Supplemental Figure S4 (A)

Supplemental Table S1. Summary of the constructs of *Sc*Nup133 and *Vp*Nup133

The chi (χ) values were computed by fitting the theoretical SAXS profile for the comparative model to the corresponding experimental SAXS profile, using FoXS (13, 14). The clones listed are all available from DNASU plasmid repository (https://dnasu.org/DNASU/Home.do).

Construct	Clone ID	Species Name	Folds	Molecular Weight (observed by ESI)	Protein ID	Chi (χ)	Qmax of the SAXS profile	Sample quality for the SAXS experiment	PDB code
55 - 502	15133f11BCt3p1	*Vanderwaltozyma polyspora*	**β-propeller**	51,628	24159	**1.14**	0.30	Good	**4Q9T**
52 - 483	15133a13BCt10p1	*Saccharomyces cerevisiae*	**β-propeller**	50,686	23911	**2.00**	0.25		
52 - 515	15133a14BCt10p1	*Saccharomyces cerevisiae*	**β-propeller**	54,270	23912	**1.25**	0.25		
41 - 483	15133a9BCt14p1	*Saccharomyces cerevisiae*	**β-propeller**	52,074	23907	**1.61**	0.25		
41 - 515	15133a10BCt3p1	*Saccharomyces cerevisiae*	**β-propeller**	55,662	23908	**1.45**	0.25	Good	
27 - 483	15133a7BCt2p1	*Saccharomyces cerevisiae*	**β-propeller**	53,694	23906	**1.61**	0.25		
27 - 515	15133a6BCt6p1	*Saccharomyces cerevisiae*	**β-propeller**	57,260	23905	**1.40**	0.25		
2 - 515	15133a2BCt11p1	*Saccharomyces cerevisiae*	**β-propeller**	60,134	23902	**1.36**	0.25		
508 - 822	15133a24BCt4p1	*Saccharomyces cerevisiae*	**α-solenoid**	38,312	23918	**1.89**	0.25		
508 - 879	15133a25BCt4p1	*Saccharomyces cerevisiae*	**α-solenoid**	45,262	23919	**1.29**	0.18		
490 - 822	15133a21BCt10p1	*Saccharomyces cerevisiae*	**α-solenoid**	40,344	23915	**1.29**	0.27	Good	
490 - 879	15133a22BCt4p1	*Saccharomyces cerevisiae*	**α-solenoid**	47,296	23916	**1.78**	0.30		
944 - 1157	15133a31BCt11p1	*Saccharomyces cerevisiae*	**α-solenoid**	25,876	23922	**1.31**	0.30		**3KFO**
521 - 1157	15133a29BCt5p1	*Saccharomyces cerevisiae*	**α-solenoid**	75,730	23921	**2.90**	0.25	Minor Aggregation	
508 - 1157	15133a26BCt14p1	*Saccharomyces cerevisiae*	**α-solenoid**	77,160	23920	**1.71**	0.30	Good	
490 - 1157	15133a23BCt4p1	*Saccharomyces cerevisiae*	**α-solenoid**	79,198	23917	**3.55**	0.24	Minor Aggregation	
41 - 879	15133a11BCt4p1	*Saccharomyces cerevisiae*	**β-propeller + α-solenoid**	99,818	24047	**3.26**	0.25		
41 - 1157	15133a12BCt7p1	*Saccharomyces cerevisiae*	**β-propeller + α-solenoid**	130,698	23910	**4.56**	0.30	Good	
2 - 1157	15133a4BCt5p1	*Saccharomyces cerevisiae*	**β-propeller + α-solenoid**	135,154	23904	**6.27**	0.25		

Supplemental Table S2. Mutational analysis of the *Sc*Nup133 - *Sc*Nup84 interface

Maximally disruptive mutations were predicted by program EGAD (15), at the target residues with large solvent accessibility change (residues of L922, L929, and L933) calculated by MODELLER (16). The values of "dddG" and "ddG_{free}" in the table are shown in kcal / mol unit.

Seq#	WT	Mutant	dddG	ddGfree
922	L	Y	76.347998	0.475281
933	L	W	67.836604	-0.148324
922	L	F	66.314425	0.331004
929	L	W	62.302957	0.341234
929	L	Y	56.962032	0.246146
926	V	W	45.684815	-5.819709
922	L	H	43.827110	0.572563
929	L	F	29.044934	0.403725
891	I	W	25.972846	-1.024380
925	N	I	19.968437	-1.017121
916	S	Y	17.529265	30.097123
933	L	R	17.120624	-0.585448
929	L	H	16.065889	0.569485
891	I	Y	15.977410	-0.920009
930	S	R	14.613645	-1.143554
922	L	Q	12.846677	0.711871
891	I	R	11.598520	-0.480485
888	I	Y	11.594024	0.164722
933	L	F	11.437325	-0.149780
930	S	K	10.885282	-0.290207
925	N	W	10.139592	-0.942144

Supplemental Table S3. Summary of the *em2D* Z-scores and cross-correlation coefficients, calculated for the multi-state model of *Sc*Nup133$^{2\text{-}1157}$

Each of the 23 EM class averages was attempted to be assigned to one or more of the 4 conformations in the multi-state model: An EM class average is assigned to a conformation when its *em2D* Z-score is less than -0.95 and the cross-correlation coefficient is higher than 0.82 or 0.85. As a result, EM class 23 was not assigned to any conformation. The assigned classes are indicated by color for each conformation.

Class ID	Images per class	Cross correlation coefficient cutoff	Conformation #1		Conformation #2		Conformation #3		Conformation #4	
			em2D Z-score	Cross correlation coefficient	*em2D* Z-score	Cross correlation coefficient	*em2D* Z-score	cross correlation coefficient	*em2D* Z-score	Cross correlation coefficient
1	103		-0.314	0.846	0.055	0.830	-0.591	0.858	-1.329	0.890
2	100		-0.497	0.832	-0.225	0.811	-0.975	0.869	-0.755	0.852
3	88		-1.659	0.907	-0.159	0.870	-1.578	0.905	-0.848	0.887
4	88	0.82	0.889	0.818	1.614	0.801	-1.635	0.877	-1.368	0.871
5	64		-1.005	0.853	-0.283	0.819	-0.043	0.808	-1.139	0.859
6	60		-0.526	0.845	-0.681	0.851	-1.105	0.869	-1.105	0.869
7	111		-0.432	0.852	0.112	0.843	-1.540	0.886	-1.901	0.898
8	88	0.85	-1.813	0.879	-1.453	0.863	-1.048	0.845	-1.925	0.884
9	51	0.82	-2.636	0.871	-2.403	0.865	-2.441	0.866	-0.108	0.806
10	70	0.85	-1.613	0.865	-1.012	0.836	-1.447	0.857	-1.219	0.846
11	49		-1.178	0.868	-1.124	0.863	-0.733	0.829	-0.923	0.846
12	100		-2.474	0.849	-2.197	0.838	-2.700	0.858	-1.391	0.806
13	32		-1.537	0.891	-1.460	0.889	-2.117	0.906	-0.879	0.874
14	76		-0.870	0.893	-0.266	0.869	-1.072	0.901	-0.907	0.894
15	77		-1.383	0.871	-0.017	0.808	-0.531	0.832	-1.111	0.859
16	44		-2.558	0.903	-2.102	0.884	-1.742	0.869	-0.637	0.823
17	56	0.82	-2.531	0.883	-2.448	0.880	-2.448	0.880	-0.350	0.804
18	86		-0.640	0.868	0.465	0.840	-0.763	0.871	-1.050	0.878
19	120		-0.492	0.851	0.074	0.820	-0.516	0.853	-1.441	0.904
20	16		-1.269	0.828	-0.882	0.795	-0.859	0.794	-1.324	0.832
21	34		-0.671	0.839	-0.197	0.825	-1.014	0.849	-0.766	0.841
22	6		-0.984	0.858	0.535	0.809	-0.054	0.828	-1.790	0.884
23	11		-0.581	0.867	0.268	0.828	-0.041	0.842	-0.819	0.878
Total	1530									
Average	66.5		-1.164	0.862	-0.599	0.841	-1.174	0.859	-1.091	0.860
Standard Deviation	32.4		0.87	0.023	1.04	0.028	0.77	0.029	0.45	0.030

Supplemental References

1. Van Duyne, G. D., Standaert, R. F., Karplus, P. A., Schreiber, S. L., and Clardy, J. (1993) Atomic structures of the human immunophilin FKBP-12 complexes with FK506 and rapamycin. *J Mol Biol* 229, 105-124

2. Kuwamoto, S., Akiyama, S., and Fujisawa, T. (2004) Radiation damage to a protein solution, detected by synchrotron X-ray small-angle scattering: dose-related considerations and suppression by cryoprotectants. *J. Synchrotron Rad.* 11, 462-468

3. McPhillips, T. M., McPhillips, S. E., Chiu, H.-J., Cohen, A. E., Deacon, A. M., Ellis, P. J., Garman, E., Gonzalez, A., Sauter, N. K., Phizackerley, R. P., Soltis, S. M., and Kuhn, P. (2002) Blu-Ice and the Distributed Control System: software for data acquisition and instrument control at macromolecular crystallography beamlines. *J Synchrotron Radiat* 9, 401-406

4. Martel, A., Liu, P., Weiss, T. M., Niebuhr, M., and Tsuruta, H. (2012) An integrated high-throughput data acquisition system for biological solution X-ray scattering studies. *J Synchrotron Radiat* 19, 431-434

5. Hura, G. L., Menon, A. L., Hammel, M., Rambo, R. P., Poole, F. L., 2nd, Tsutakawa, S. E., Jenney, F. E., Jr., Classen, S., Frankel, K. A., Hopkins, R. C., Yang, S. J., Scott, J. W., Dillard, B. D., Adams, M. W., and Tainer, J. A. (2009) Robust, high-throughput solution structural analyses by small angle X-ray scattering (SAXS). *Nat Methods* 6, 606-612

6. Li, Z., Hite, R. K., Cheng, Y., and Walz, T. (2010) Evaluation of imaging plates as recording medium for images of negatively stained single particles and electron diffraction patterns of two-dimensional crystals. *J Electron Microsc (Tokyo)* 59, 53-63

7. Ludtke, S. J., Baldwin, P. R., and Chiu, W. (1999) EMAN: semiautomated software for high-resolution single-particle reconstructions. *J Struct Biol* 128, 82-97

8. Yang, Z., Fang, J., Chittuluru, J., Asturias, F. J., and Penczek, P. A. (2012) Iterative stable alignment and clustering of 2D transmission electron microscope images. *Structure* 20, 237-247

9. Weinkam, P., Pons, J., and Sali, A. (2012) Structure-based model of allostery predicts coupling between distant sites. *Proc Natl Acad Sci U S A* 109, 4875-4880

10. Pettersen, E. F., Goddard, T. D., Huang, C. C., Couch, G. S., Greenblatt, D. M., Meng, E. C., and Ferrin, T. E. (2004) UCSF Chimera--a visualization system for exploratory research and analysis. *J Comput Chem* 25, 1605-1612

11. Gautier, R., Douguet, D., Antonny, B., and Drin, G. (2008) HELIQUEST: a web server to screen sequences with specific alpha-helical properties. *Bioinformatics* 24, 2101-2102

12. Devos, D., Dokudovskaya, S., Williams, R., Alber, F., Eswar, N., Chait, B. T., Rout, M. P., and Sali, A. (2006) Simple fold composition and modular architecture of the nuclear pore complex. *Proc Natl Acad Sci U S A* 103, 2172-2177

13. Schneidman-Duhovny, D., Hammel, M., and Sali, A. (2010) FoXS: a web server for rapid computation and fitting of SAXS profiles. *Nucleic Acids Res* 38, W540-544

14. Schneidman-Duhovny, D., Hammel, M., Tainer, J. A., and Sali, A. (2013) Accurate SAXS profile computation and its assessment by contrast variation experiments. *Biophys J* 105, 962-974

15. Pokala, N., and Handel, T. M. (2005) Energy functions for protein design: adjustment with protein-protein complex affinities, models for the unfolded state, and

negative design of solubility and specificity. *J Mol Biol* 347, 203-227

16. Sali, A., and Blundell, T. L. (1993) Comparative protein modelling by satisfaction of spatial restraints. *J Mol Biol* 234, 779-815